Chinese Journal of Mechanical Engineering

ORIGINAL ARTICLE

Open Access

An Improved Time-Domain Inverse Technique for Localization and Quantification of Rotating Sound Sources

Xiaozheng Zhang[1*], Yinlong Li[2], Yongbin Zhang[1], Chuanxing Bi[1], Jinghao Li[3] and Liang Xu[1]

Abstract

The time-domain inverse technique based on the time-domain rotating equivalent source method has been proposed to localize and quantify rotating sound sources. However, this technique encounters two problems to be addressed: one is the time-consuming process of solving the transcendental equation at each time step, and the other is the difficulty of controlling the instability problem due to the time-varying transfer matrix. In view of that, an improved technique is proposed in this paper to resolve these two problems. In the improved technique, a de-Dopplerization method in the time-domain rotating reference frame is first applied to eliminate the Doppler effect caused by the source rotation in the measured pressure signals, and then the restored pressure signals without the Doppler effect are used as the inputs of the time-domain stationary equivalent source method to locate and quantify sound sources. Compared with the original technique, the improved technique can avoid solving the transcendental equation at each time step, and facilitate the treatment of the instability problem because the transfer matrix does not change with time. Numerical simulation and experimental results show that the improved technique can eliminate the Doppler effect effectively, and then localize and quantify the rotating nonstationary or broadband sources accurately. The results also demonstrate that the improved technique can guarantee a more stable reconstruction and compute more efficiently than the original one.

Keywords Rotating sound sources, De-Dopplerization, Time-domain equivalent source method

1 Introduction

Rotating sound sources, for example the fans, are often encountered in our daily lives and the industrial fields. Localization and quantification of rotating sound sources based on the microphone array measurements is helpful to analyze source generation mechanisms and predict their radiated sound fields. A series of microphone array methods have been developed to realize this aim. In these methods, the microphone array is usually fixed in the sound fields because a synchronously rotating microphone array with sources will produce the strong aerodynamic noise and bring the great installation difficulty. However, the relative motion between the fixed microphone array and the rotating sources leads to the Doppler effect that causes the amplitude distortion and frequency offset of real acoustic signals. If the Doppler effect is not eliminated, the erroneous localization and quantification results will be obtained. Therefore, the treatment of the Doppler effect has always been a topic in the microphone array methods for the localization and quantification of rotating sound sources.

To eliminate the Doppler effect, Lowis and Joseph [1, 2] developed a frequency-domain rotating reference

*Correspondence:
Xiaozheng Zhang
xzhengzhang@hfut.edu.cn
[1] Institute of Sound and Vibration Research, Hefei University of Technology, Hefei 230009, China
[2] Volkswagen (Anhui) Automotive Company Limited, Hefei 230000, China
[3] East China Electric Power Test & Research Institute, China Datang Corporation Science and Technology General Research Institute Co. LTD, Hefei 230088, China

frame in which the virtual microphones are rotating synchronously with sound sources. The pressure spectra at the positions of virtual rotating microphones were obtained from the spinning mode decomposition of pressure spectra measured by the actual fixed microphones. Since the virtual microphone data is prevented from the Doppler effect, it can be directly used as the input of the frequency-domain beamforming or inverse method to locate rotating sound sources [1–6].

Dougherty et al. [7] and Jekosch et al. [8, 9] employed a time-domain interpolation method to eliminate the Doppler effect. It also assumes that the virtual microphones are rotating synchronously with sound sources. The temporal pressure signals at the positions of virtual rotating microphones are linearly interpolated between the measured pressure signals at neighboring actual fixed microphones. Ma et al. [10] investigated the relationship between the cross-spectral matrices obtained by the frequency-domain rotating reference frame and the time-domain interpolation method, and analyzed their advantages and disadvantages in detail. In particular, they concluded that the essence of the frequency-domain rotating reference frame is to calculate the pressure at each virtual rotating microphone through the Fourier interpolation on the sound pressures at all actual microphones.

Other than eliminating the Doppler effect, Sijtsma et al. [11, 12] incorporated the Doppler effect into a transfer function relating the strengths of rotating sound sources at the source time to the pressures at the positions of actual fixed microphones at the receiver time. They used the transfer function to construct the steering vector and then developed the time-domain rotating beamforming (TRB) for locating rotating sound sources. Minck et al. [13] and Amoiridis et al. [14] used the TRB to locate rotating sources on the blades of a fan. Ma et al. [15] analyzed the ghost contribution in the TRB due to the Doppler effect in virtue of a detailed theoretical derivation, and provided an effective strategy to compensate the Doppler effect in the TRB. Pan et al. [16] developed a correction method for the TRB to restrain the singular problem in identifying rotating sources with the non-uniform directivity. In recent years, deconvolution algorithms were subsequently used to improve the spatial resolution of the TRB [17–21]. Nevertheless, the TRB utilizes the advanced time method to calculate the receiver time based on the source time, which causes inconsistency between the calculated receiver time and the sampling time. Consequently, the oversampling and interpolation of microphone signals are needed to deal with the inconsistency problem.

Zhang et al. [22, 23] also incorporated the Doppler effect into the transfer function, but developed a time-domain inverse technique based on the time-domain rotating equivalent source method (TRESM) to locate and quantify rotating sound sources. The time-domain inverse technique employs the retarded time method to calculate the source time based on the sampling time, thus avoiding the oversampling and interpolation of microphone signals. However, the calculation of the source time based on the sampling time is to solve the transcendental equation in a numerical iterative scheme, and the calculation has to be done for each time, so the time-domain inverse technique is time-consuming. Moreover, the time-domain inverse technique suffers from the instability that is caused by the use of the time marching scheme in the TRESM. The instability is closely related to the ill-posed transfer matrix. Since the equivalent sources are given to be rotating in the time-domain inverse technique, the transfer matrix varies with time, which leads to the difficulty of dealing with the instability problem.

In this paper, the time-domain inverse technique is improved to address the time-consuming and instability problems caused by the use of the TRESM. In the improved technique, a de-Dopplerization method in the time-domain rotating reference frame is first applied to eliminate the Doppler effect caused by source rotation, and then the time-domain stationary equivalent source method (TSESM) is used to locate and quantify sound sources. The joint application of the de-Dopplerization method and TSESM will avoid solving the transcendental equation at each time step, and facilitate the treatment of the instability problem according to the time-invariant property of the transfer matrix.

2 Theory

As shown in Figure 1, a sound source is assumed to rotate with an angular velocity Ω around the z-axis, and a ring array containing N evenly spaced microphones is fixed in the field and used to measure pressure signals.

Due to the relative motion between the source and microphones, the pressure signals measured by the microphones are contaminated by the Doppler effect. If the microphones are made to rotate virtually with the source at the same angular velocity Ω, the pressures at the positions of the virtual rotating microphones are free from the Doppler effect. Through the Fourier interpolation from the pressures at all actual microphones, the pressure $p(\varphi, t)$ at any circumferential position on the microphone ring can be expressed as

$$p(\varphi, t) = \sum_{m=-|1-N|/2}^{N/2} P(m, t) e^{\mathrm{i}m\varphi}, \tag{1}$$

where m is the spinning mode order, and $P(m, t)$ is the spinning mode amplitude that can be determined by

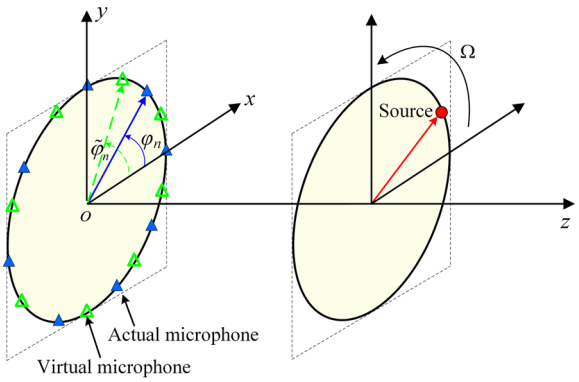

Figure 1 The rotating sound source, the actual microphones and the virtual rotating microphones

$$P(m,t)=\frac{1}{N}\sum_{n=1}^{N}p(\varphi_n,t)e^{-\mathrm{i}m\varphi_n}. \tag{2}$$

In Eq. (2), $p(\varphi_n,t)$ is the pressure measured by the nth actual microphone. For the nth virtual rotating microphone, the circumferential position on the microphone ring at the instant t can be obtained as

$$\tilde{\varphi}_n=\varphi_n+\Omega t. \tag{3}$$

By substituting Eq. (3) into Eq. (1), the pressure at the position of the nth virtual rotating microphone can be then calculated as

$$p(\tilde{\varphi}_n,t)=\sum_{m=-|1-N|/2}^{N/2}P(m,t)e^{\mathrm{i}m(\varphi_n+\Omega t)}. \tag{4}$$

Equation (4) is the de-Dopplerization formulation in the time-domain rotating reference frame, which is an extension of the de-Dopplerization formulation in the frequency-domain rotating reference frame proposed by Lowis and Joseph [1, 2] and was firstly given by Ma et al. [10]. It indicates that the pressures free from the Doppler effect can be obtained by processing the pressures measured by a fixed microphone array. Note that Eq. (4) is operated at each sampling time, and thus it is particularly applicable to nonstationary signals and broadband signals in practical engineering.

In the time-domain rotating reference frame, the virtual microphones are rotating synchronously with the sources. If the effect of the rotating medium is ignored, the system of rotating sources and virtual rotating microphones can be transformed into the system of stationary sources and stationary microphones. After the pressures $p(\tilde{\varphi}_n,t)$ with $n=1,\ 2,\ \cdots,\ N$ at the positions of virtual rotating microphones have been extracted in the previous subsection, they are used as the inputs of TSESM.

In the generalized time-domain equivalent source method, the temporal pressure $p_n(t)$ radiated from the actual sources at the nth measurement point can be modeled by summing the contributions of a series of equivalent sources located on the source plane [24–26], that is

$$p_n(t)=\sum_{l=1}^{L}q_l(\tau)g_{nl},\quad n=1,\ 2,\ \cdots,\ N, \tag{5}$$

where t and τ are defined as the receiver and source times, respectively, l indicates the lth equivalent source, L is the number of equivalent sources, $q(\tau)$ is the equivalent source strength as a function of source time, and g_{nl} is the transfer function given by

$$g_{nl}=\frac{1}{4\pi R_{nl}}, \tag{6}$$

where R_{nl} is the distance between the nth measurement point and the lth equivalent source.

Discretizing the receiver time and source time as $t^i,\ i=1,\ 2,\ \cdots,\ I$ and $\tau^j,\ j=1,\ 2,\ \cdots,\ J$ with the uniform intervals Δt and $\Delta\tau$, and introducing the linear interpolation function $\phi^j(\tau)$ [27, 28], i.e.,

$$\phi^j(\tau)=\begin{cases}(\tau-\tau^{j-1})/\Delta\tau, & \text{when } (\tau^{j-1}\le\tau\le\tau^j),\\ (\tau^{j+1}-\tau)/\Delta\tau, & \text{when } (\tau^j\le\tau\le\tau^{j+1}),\\ 0, & \text{otherwise,}\end{cases} \tag{7}$$

to the equivalent source strength, a matrix equation for each receiver time step can be derived as

$$\boldsymbol{P}^i=\sum_{j=1}^{i}\boldsymbol{G}^{ij}\boldsymbol{Q}^j, \tag{8}$$

where $\boldsymbol{P}^i$ is a column vector composed of $p_n(t^i)$ with $n=1,\ 2,\ \cdots,\ N$, $\boldsymbol{Q}^j$ is a column vector composed of $q_l(\tau^j)$ with $l=1,\ 2,\ \cdots,\ L$ and the transfer matrix $\boldsymbol{G}^{ij}$ of size $N\times L$ can be expressed as

$$\boldsymbol{G}^{ij}(n,l)=\frac{\phi^j(\tau^i_{nl})}{4\pi R_{nl}}, \tag{9}$$

with $\tau^i_{nl}=t^i-R_{nl}/c$.

Based on Eq. (8), an iterative process of solving the equivalent source strengths can be derived as

$$\boldsymbol{Q}^i=(\boldsymbol{G}^{ii})^{+}(\boldsymbol{P}^i-\boldsymbol{G}^{i1}\boldsymbol{Q}^1-\boldsymbol{G}^{i2}\boldsymbol{Q}^2-\cdots-\boldsymbol{G}^{i(i-1)}\boldsymbol{Q}^{i-1}), \tag{10}$$

where the superscript "+" indicates the pseudo inverse of a matrix.

For the TRESM depicted in Ref. [22], since the equivalent sources are supposed to be rotating with the actual sources and the microphone array is fixed, the

distance R_{nl} between the nth microphone and the lth equivalent source is time-dependent and has

$$R_{nl}(\tau_{nl}^i) = \sqrt{(z_n - z_l)^2 + r_n^2 + r_l^2 + 2r_n r_l \cos(\Omega\tau_{nl}^i + \varphi_{l0} - \varphi_n)}, \tag{11}$$

where the coordinates (r_n, φ_n, z_n) indicate the position of the nth microphone, and the coordinates (r_l, φ_{l0}, z_l) indicate the initial position of the lth equivalent source. It is seen from Eq. (11) that the time-dependent distance $R_{nl}(\tau_{nl}^i)$ can be calculated only when the source time τ_{nl}^i is known in advance. In fact, the source time τ_{nl}^i should be determined at each time step by solving the transcendental equation

$$c(t^i - \tau_{nl}^i) = R_{nl}(\tau_{nl}^i). \tag{12}$$

Note that Eq. (12) cannot be solved analytically, and thus a numerical iterative scheme has to be used to obtain its roots, which results in a time-consuming calculation when performing the TRESM. Moreover, the time-dependent R_{nl} results in the transfer matrix to be inverted, $\boldsymbol{G}^{ii}$, varying with the time step. Considering that the transfer matrix $\boldsymbol{G}^{ii}$ is generally ill-posed, which is the main cause of the instability problem, the Tikhonov regularization and time averaging method are used at each time step to guarantee the appropriate solution of equivalent source strengths. However, it should be mentioned that the Tikhonov regularization cannot always guarantee an effective filtering at each time step due to the improper regularized parameters chosen by the generalized crossed validation method, especially in the cases of strong noise contained in the measured pressure and inappropriate selection of numerical parameters, and furthermore time averaging method can only play an assistant role in attenuating the instability. Therefore, the instability problem still exists in some cases, which is a serious defect owned by the TRESM.

However, for the TSESM, the distance R_{nl} is constant for each time step due to the configuration of synchronously rotating equivalent sources and virtual microphones, and it can be calculated analytically as

$$R_{nl} = \sqrt{(z_n - z_l)^2 + r_n^2 + r_l^2 + 2r_n r_l \cos(\varphi_{l0} - \tilde{\varphi}_{n0})}, \tag{13}$$

where the coordinates $(r_n, \tilde{\varphi}_{n0}, z_n)$ indicate the initial position of the nth virtual microphone. Note that the calculation of the source time is not needed to determine the distance R_{nl} in the TSESM, thus avoiding the time-consuming process of solving the transcendental equation at each time step. Moreover, the constant R_{nl} gives the linear interpolation function an important property, i.e.,

$$\phi^j(\tau_{nl}^i) = \phi^{j-1}(\tau_{nl}^{i-1}) = \phi^{j-2}(\tau_{nl}^{i-2}) = \cdots = \phi^1(\tau_{nl}^{i-j+1}). \tag{14}$$

Based on the property, it further yields

$$\boldsymbol{G}^{ij} = \boldsymbol{G}^{(i-1)(j-1)} = \boldsymbol{G}^{(i-2)(j-2)} = \cdots = \boldsymbol{G}^{(i-j+1)(1)}. \tag{15}$$

From Eq. (15), it can be concluded that the transfer matrix to be inverted $\boldsymbol{G}^{ii}$ is constant at each time step. Accordingly, Eq. (8) can be rewritten as

$$\boldsymbol{P}^i = \sum_{j=1}^{i} \boldsymbol{G}^{i-j+1}\boldsymbol{Q}^j, \tag{16}$$

with

$$\boldsymbol{G}^{i-j+1}(n,l) = \frac{\phi^1(\tau_{nl}^{i-j+1})}{4\pi R_{nl}}. \tag{17}$$

According to the finiteness of nonzero interval in the linear interpolation function, Eq. (16) can be rewritten as [29, 30]

$$\boldsymbol{P}^i = \sum_{k=1}^{K} \boldsymbol{G}^k \boldsymbol{Q}^{i-k+1}. \tag{18}$$

In Eq. (18), it has

$$K = \frac{1}{c\Delta\tau}(R_{\max} - R_{\min}) + 2, \tag{19}$$

where $R_{\max}$ and $R_{\min}$ are the maximum and minimum distances between equivalent sources and measurement points. Based on Eq. (18), the iterative process of solving the equivalent source strengths can be derived as

$$\boldsymbol{Q}^i = (\boldsymbol{G}^1)^+(\boldsymbol{P}^i - \boldsymbol{G}^2\boldsymbol{Q}^{i-1} - \boldsymbol{G}^3\boldsymbol{Q}^{i-2} - \cdots - \boldsymbol{G}^K\boldsymbol{Q}^{i-K+1}). \tag{20}$$

In a large iterative scheme, Eq. (20) can be rewritten as

$$\boldsymbol{Y}^i = \boldsymbol{H}\boldsymbol{Y}^{i-1} + \boldsymbol{X}^i, \tag{21}$$

where

$$\boldsymbol{Y}^i = \begin{bmatrix} \boldsymbol{Q}^i \\ \boldsymbol{Q}^{i-1} \\ \vdots \\ \boldsymbol{Q}^{i-K+3} \\ \boldsymbol{Q}^{i-K+2} \end{bmatrix}, \boldsymbol{Y}^{i-1} = \begin{bmatrix} \boldsymbol{Q}^{i-1} \\ \boldsymbol{Q}^{i-2} \\ \vdots \\ \boldsymbol{Q}^{i-K+2} \\ \boldsymbol{Q}^{i-K+1} \end{bmatrix}, \boldsymbol{X}^i = \begin{bmatrix} (\boldsymbol{G}^1)^+\boldsymbol{P}^i \\ \boldsymbol{0} \\ \vdots \\ \boldsymbol{0} \\ \boldsymbol{0} \end{bmatrix}, \tag{22}$$

and

$$\boldsymbol{H}=\begin{bmatrix} -\left(\boldsymbol{G}^1\right)^+\boldsymbol{G}^2 & \cdots & -\left(\boldsymbol{G}^1\right)^+\boldsymbol{G}^{K-1} & -\left(\boldsymbol{G}^1\right)^+\boldsymbol{G}^K \\ \boldsymbol{I} & & \boldsymbol{0} & \boldsymbol{0} \\ & \ddots & & \vdots \\ \boldsymbol{0} & \cdots & \boldsymbol{I} & \boldsymbol{0} \end{bmatrix}, \tag{23}$$

Note that the iterative matrix $\boldsymbol{H}$ is time-invariant due to the invariant $\boldsymbol{G}^1$, $\boldsymbol{G}^2$, $\cdots$, $\boldsymbol{G}^K$ at each iteration. In the viewpoint of system theory, the stability of this time-invariant system is determined by the eigenvalues decomposed from $\boldsymbol{H}$. The stability condition requires that the maximum magnitude of eigenvalues should not be larger than one [30]. Based on the stability condition, the stabilization method based on the Tikhonov regularization and the time averaging can be improved by using the classical golden section method to search the regularization parameter for satisfying the stability condition. The improved stabilization method can always keep the stable results. The detailed analysis can be found in Ref. [30]. Here, it should be pointed out that Eq. (10) deduced in the TRESM cannot be transformed into a similar form as Eq. (21) that has the time-invariant iterative matrix $\boldsymbol{H}$, because the transfer matrices in Eq. (10) varies with time. Therefore, the improved stabilization method cannot be applied to the TRESM.

3 Numerical Simulations

A schematic of numerical simulations is shown in Figure 2. The sound sources are two rotating monopoles with the rotational frequency $f_r = 60$ Hz. Their initial positions are S_1(0.2 m, 0 rad, 0.03 m) and S_2(0.2 m, π rad, 0.03 m) in the cylindrical coordinates $o(r, \phi, z)$. Since the time-domain method is applicable to nonstationary signals and broadband signals, both cases are to be considered. In these two cases, the sampling time interval is set as $\Delta t = 1/12800$ s, and the sampling number is set as $I = 256$. In the nonstationary case, S_1 and S_2 generate the signal with a linear frequency modulation in the band of $[f_l, f_h]$ and a Gaussian amplitude modulation. This signal can be described with the following equation

$$s(t_i) = \cos\left[2\pi f_l(t_i - t_c) + 2\pi(f_h - f_l)\frac{(t_i - \Delta t)^2 - (t_c - \Delta t)^2}{2(I-1)\Delta t}\right] \times e^{-\pi[(t_i - t_c)/a]^2}. \tag{24}$$

Where f_l and f_h are the initial and final frequencies of the linear frequency modulation, respectively. Their values are given as $[f_l, f_h] = [300, 700]$ Hz for S_1, and $[f_l, f_h] = [1300, 1700]$ Hz for S_2. t_c is the time delay, given as $t_c = 320\Delta t$. a is the time spreading width, given as $a = 200\Delta t$. In the broadband case, S_1 and S_2 emit the amplitude-modulated broadband signal with the equation as follows:

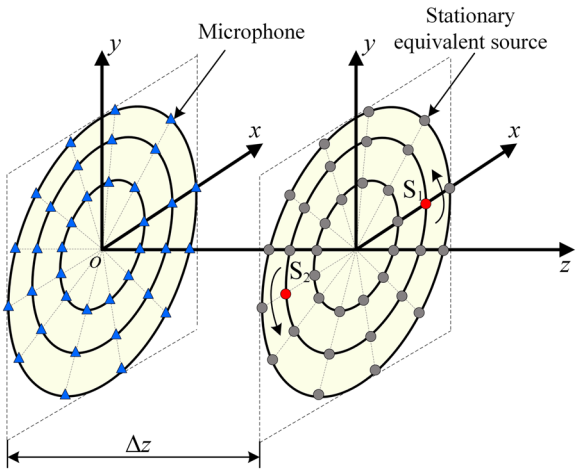

Figure 2 Geometric description of two rotating sound sources S_1 and S_2, the distributions of equivalent sources and measurement points

$$s(t_i) = \cos(2\pi f_c t_i)\sum_{j=1}^{J}\cos[2\pi \boldsymbol{f}(j)t_i + \boldsymbol{b}(j)\pi], \tag{25}$$

where f_c is the carrier frequency for the amplitude modulation, given as $f_c = 1000$ Hz. $\boldsymbol{f}$ is a vector containing the uniformly discretized frequencies in the given frequency band of [0, 6400] Hz. The discrete interval is 100 Hz. $\boldsymbol{b}$ is a vector containing a random permutation of the integers from 1 to J inclusive. J is given as 65.

The microphone array contains three rings with the radii of 0.1 m, 0.2 m and 0.3 m, and each ring contains twelve microphones. The distance between the microphone array and the source plane is set as $\Delta z = 0.03$ m. In order to model the actual measurement, the Gaussian white noise with the signal-to-noise ratio of 30 dB is added to the signal measured by each microphone.

The de-Dopplerization method in the time-domain rotating reference frame is used to each ring of microphones. Here, we choose the outer ring to display the results. Figure 3 presents the pressure signals and the corresponding spectra at the measurement point of (0.3 m, 5π/6 rad, 0 m) in the nonstationary case. By comparing the pressure signals and their spectra radiated by stationary sound sources (solid lines) to those radiated

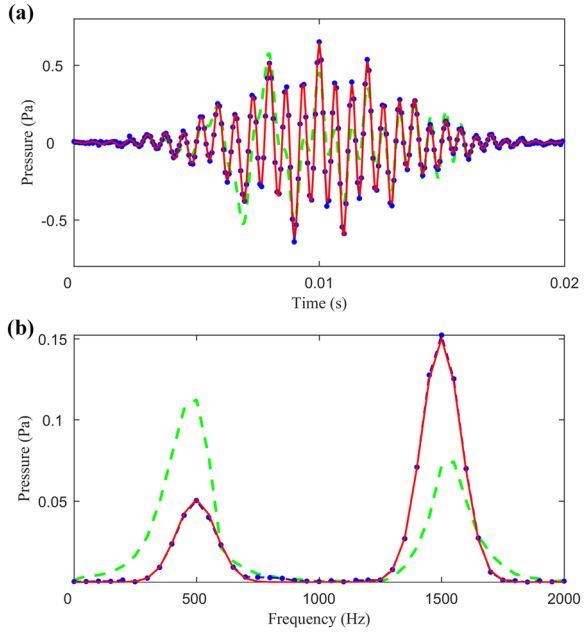

Figure 3 (**a**) The pressure signals and (**b**) the corresponding spectra radiated by stationary sound sources (solid lines), radiated by rotating sound sources (dashed lines) and obtained by using the de-Dopplerization method (dashed lines with solid points) at the measurement point of (0.3 m, 5π/6 rad, 0 m) in the nonstationary case

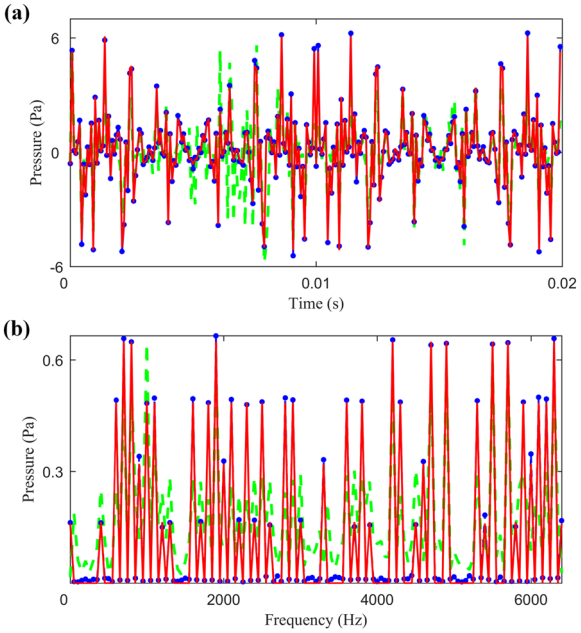

Figure 4 (**a**) The pressure signals and (**b**) the corresponding spectra radiated by stationary sources (solid lines), radiated by rotating sound sources (dashed lines) and obtained by using the de-Dopplerization method (dashed lines with solid points) at the measurement point of (0.3 m, 5π/6 rad, 0 m) in the broadband case

by rotating sound sources (dashed lines), it can be found that the Doppler effect caused by the source rotation changes pressures significantly in both time and frequency domains. By comparing the signals and their spectra radiated by stationary sources (solid lines) to those obtained by using the de-Dopplerization method (dotted lines), it is seen that the use of de-Dopplerization method can eliminate the Doppler effect effectively and recover the signals as radiated by stationary sources. The similar conclusions can be drawn in the broadband case, as shown in Figure 4, where the pressure signals and the corresponding spectra are displayed in the same measurement point as the nonstationary case.

After eliminating the Doppler effect, the rotating sound sources can be treated as the stationary ones. Then, the localization process is performed by applying the TSESM. The setup of stationary equivalent sources is shown in Figure 2. They are distributed on three rings with the radii of 0.1 m, 0.2 m and 0.3 m on the source plane, and each ring contains twelve stationary equivalent sources. In the TSESM, the strengths of stationary equivalent sources are solved at each time step. The peaks of stationary equivalent source strengths at each time step are used to indicate the positions of actual sources. Here, it should be noted that the indicated positions of actual sources are to be constant at each time step since the rotating actual sources have been transformed into the stationary ones. In fact, the indicated positions are corresponding to the initial positions of rotating actual sources. In order to concisely display the localization results, an energy average of the solved strengths at all time steps for each stationary equivalent source is calculated as

$$\overline{q}_l = \sqrt{\sum_{j=1}^{J} |q_{j,l}|^2 \Big/ J}, \tag{26}$$

where $q_{j,l}$ denotes the strength of the lth equivalent source at the jth time step.

Figure 5(a) and (c) show the localization results by using the pressures after eliminating the Doppler effect as the inputs of TSESM in both nonstationary and broadband cases, while Figure 5(b) and (d) show the results by using the pressures without eliminating the Doppler effect as the inputs. It can be seen that the former results provide the clear and precise positions of rotating sound sources, which verifies the validation of the proposed approach. While the latter results seem to be rings of source strength, since motion blur smears the sources in the circumferential direction, which demonstrates the necessity of eliminating the Doppler effect.

Except to locate sound sources, the proposed approach can reconstruct the time-evolving strengths of actual sources. Taking the source S_1 as an example, Figure 6

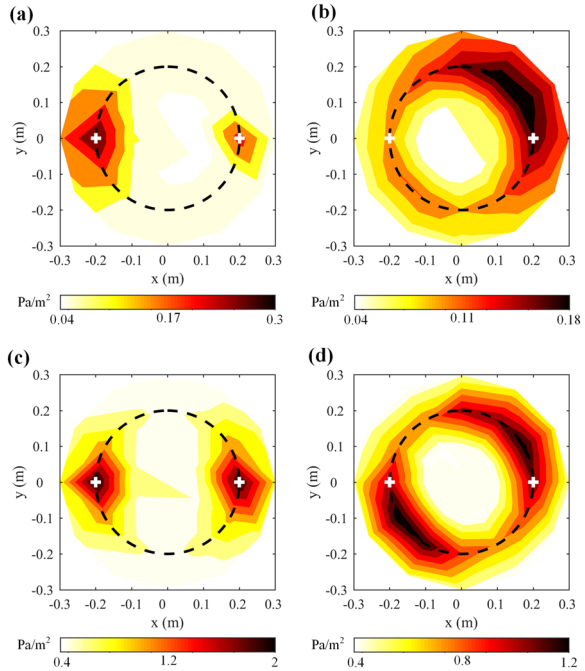

Figure 5 The localization results obtained by using the pressures after eliminating the Doppler effect as the inputs of TSESM in the nonstationary (**a**) and broadband (**c**) cases vs. those obtained by using the pressures without eliminating the Doppler effect as the inputs in the nonstationary (**b**) and broadband (**d**) cases (The plus signs indicate the positions of two rotating monopoles, and the dashed circle indicates the rotating path of monopoles)

shows the comparison of its theoretical and reconstructed strengths in both nonstationary and broadband cases. Although the proposed approach underestimates the source strengths due to the requirement of dealing with the instability problem, it achieves the agreement of time-evolving trend.

However, under the same benchmark, the TRESM is hard to obtain the stable solutions. As shown in Figure 7, the reconstructed strengths in both nonstationary and broadband cases are divergent. Moreover, the TRESM is inefficient due to the time-consuming process of solving the transcendental equation at each time step. Although the de-Dopplerization and stability process are needed when using the proposed approach, the time they consumed is relatively much less than the cost of solving the transcendental equation at each time step. In these two simulation cases, the time consumed by the proposed approach is 2.17 s and 2.34 s, while the TRESM costs 10.15 s and 10.64 s.

4 Experimental Study

Experiments were performed in a semi-anechoic chamber to further verify the applicability of the improved time-domain inverse technique. The experimental setup is shown in Figure 8. The source was one rotating loudspeaker. Note that the other loudspeaker in Figure 8 was just used to adjust the balance of motion,

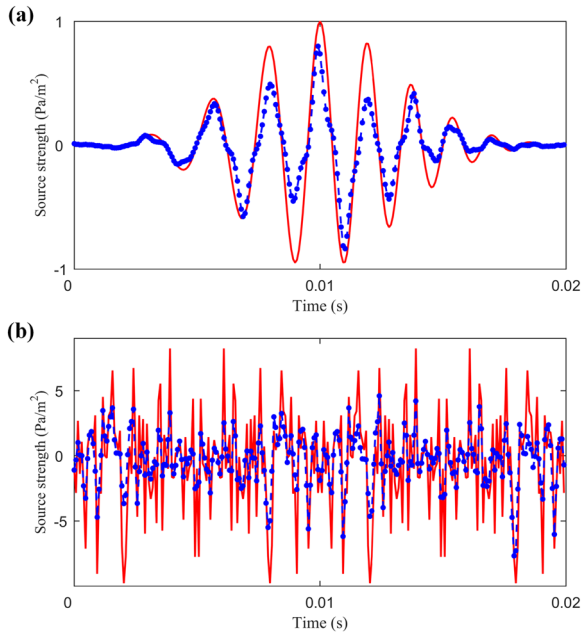

Figure 6 Time-evolving source strengths of the source S_1 in (**a**) the nonstationary case and (**b**) the broadband case: true values (solid lines), values calculated by the proposed approach (dashed lines with solid points)

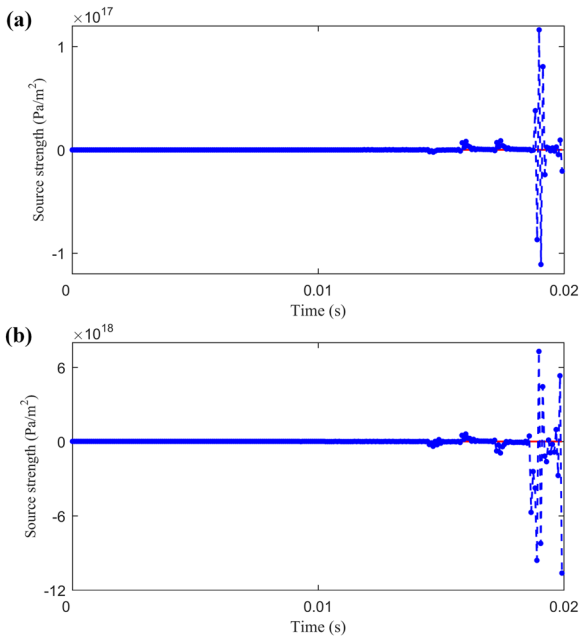

Figure 7 Time-evolving source strengths of the source S_1 in (**a**) the nonstationary case and (**b**) the broadband case: true values (solid lines), values calculated by the TRESM (dashed lines with solid points)

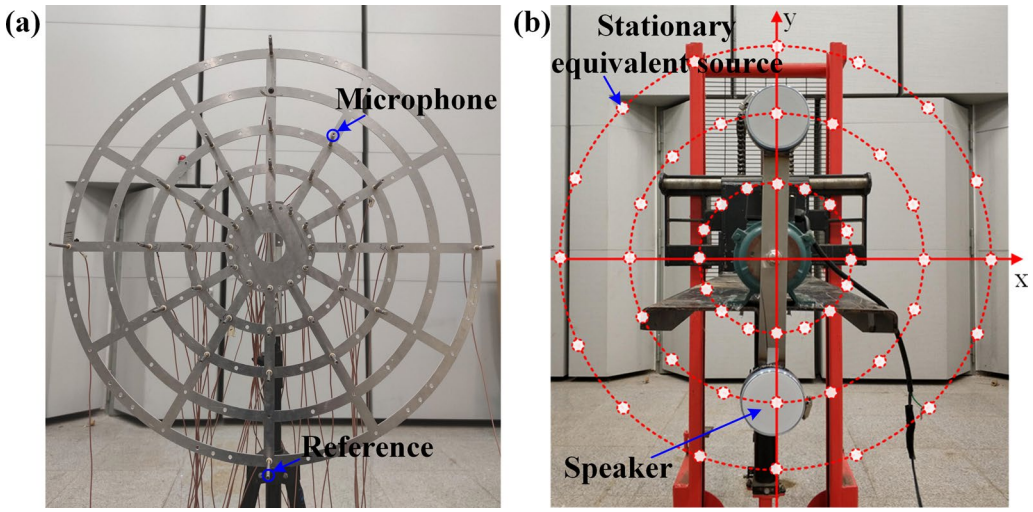

Figure 8 Experimental setup: (**a**) the microphone array, (**b**) the rotating loudspeakers and the distribution of stationary equivalent sources

and it did not generate noise. The rotational frequency f_r was set as 6 Hz, and the rotational radius (i.e., the distance from the loudspeaker center to the rotational center) was 0.16 m. The microphone array consisted of three rings with the radii of 0.08 m, 0.16 m and 0.24 m, and each ring contained twelve microphones. The microphone array was placed 0.05 m away from the rotation plane. In addition, the sampling frequency was set as 4096 Hz.

Two cases were investigated, including the nonstationary signal and broadband signal radiated by the loudspeaker. In the nonstationary case, the loudspeaker emitted the signal with a linear frequency modulation in the band of $[f_l, f_h]$ and a Gaussian amplitude modulation, as described by Eq. (24). The band was given as $[f_l, f_h] = [300, 700]$ Hz. The time delay was given as $t_c = 0.25$ s. The time spreading width was given as $a = 0.17$ s. In the broadband case, the input to the loudspeaker was the amplitude-modulated broadband signal, as described by Eq. (25). The carrier frequency was 700 Hz. The frequency band was [500, 1000] Hz.

A microphone located at (0.24 m, π/6 rad, 0 m) was selected to display the de-Dopplerization results. Figures 9 and 10 present the pressure signals and their spectra in the nonstationary and broadband cases, respectively. In these two figures, the pressure signals and their spectra were radiated by the stationary loudspeaker (solid lines), radiated by the rotating loudspeaker (dashed lines), and obtained by using the de-Dopplerization method (dashed lines with solid points). Among the comparisons of these pressure signals and spectra, it can be found that the Doppler effect caused by the source rotation changes pressures

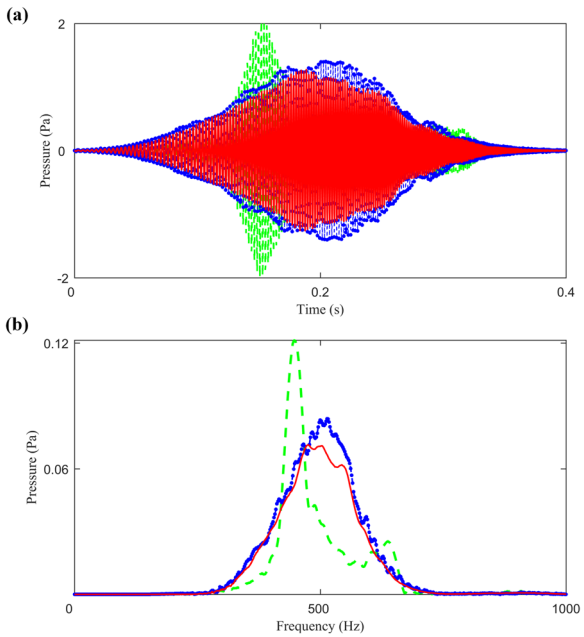

Figure 9 (**a**) The pressure signals and (**b**) the corresponding spectra radiated by the stationary loudspeaker (solid lines), radiated by the rotating loudspeaker (dashed lines), and obtained by using the de-Dopplerization method (dashed lines with solid points) at the measurement point of (0.24 m, π/6 rad, 0 m) in the nonstationary case

significantly in both time and frequency domains, and the de-Dopplerization method can eliminate the Doppler effect effectively.

After eliminating the Doppler effect, the restored pressure signals were used as the inputs of TSESM. The stationary equivalent sources were distributed on three

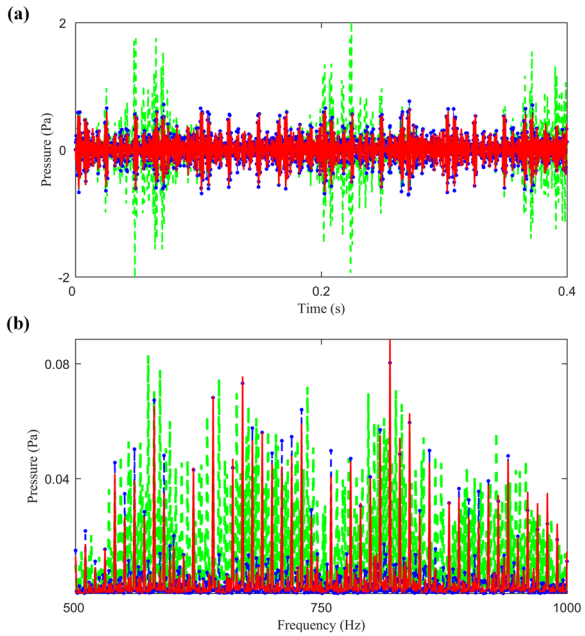

Figure 10 (**a**) The pressure signals and (**b**) the corresponding spectra radiated by the stationary loudspeaker (solid lines), radiated by the rotating loudspeaker (dashed lines), and obtained by using the de-Dopplerization method (dashed lines with solid points) at the measurement point of (0.24 m, π/6 rad, 0 m) in the broadband case

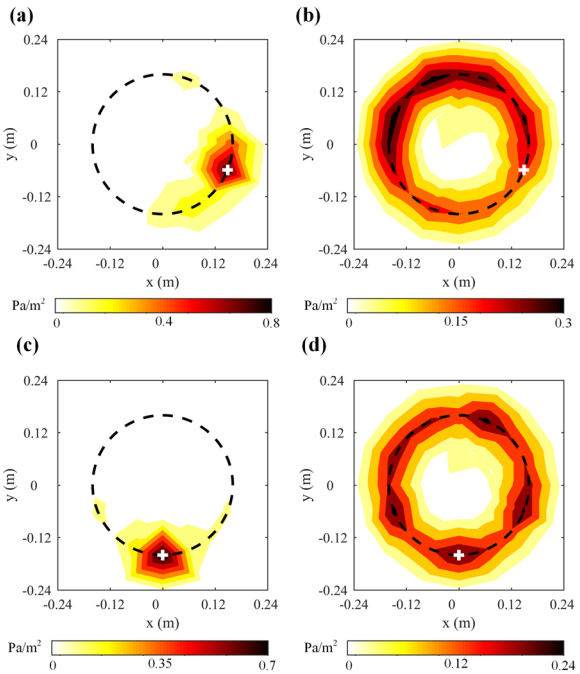

Figure 11 The localization results obtained by using the pressures after eliminating the Doppler effect as the inputs of TSESM in the nonstationary (**a**) and broadband (**c**) cases vs. those obtained by using the pressures without eliminating the Doppler effect as the inputs in the nonstationary (**b**) and broadband (**d**) cases (The plus signs indicate the position of the rotating loudspeaker, and the dashed circle indicates the rotating path of the loudspeaker)

rings with the radii of 0.08 m, 0.16 m and 0.24 m, and each ring contained sixteen equivalent sources. The energy average of the solved equivalent source strengths in time was used to display the localization results. Figure 11(a) and (c) show the localization results by using the pressures after eliminating the Doppler effect as the inputs of TSESM in the nonstationary and broadband cases, respectively. Figure 11(b) and (d) show the relevant results by using the pressures without eliminating the Doppler effect as the inputs. Obviously, the Doppler effect contaminates the localization results, however, by eliminating the Doppler effect, the position of the rotating loudspeaker can be located accurately based on the TSESM.

In addition to the localization of the rotating loudspeaker, the improved technique can realize the quantification of time-evolving strength of the loudspeaker. Since the true strength of the loudspeaker is difficult to measure experimentally, a reference point located at (0.4 m, 3π/2 rad, 0 m), as shown in Figure 8(a), was selected to compare the measured pressure and the pressure predicted by using the reconstructed source strength. This way can estimate the reconstruction accuracy of source strength indirectly. Figure 12 shows the comparisons in the nonstationary and broadband cases. The consistency between the measured and predicted pressures was acquired, which implies that the improved technique can quantify the source strength effectively.

For the same reference point, Figure 13 presents the pressures predicted by using the TRESM in both nonstationary and broadband cases. It is seen that the predicted signals are divergent. From the results shown in Figure 12 and Figure 13, it is concluded that the improved technique can guarantee a more stable reconstruction than the TRESM. Moreover, the improved technique is more efficient than the TRESM. For instance in the experiments, the time consumed by the improved technique is 6.98 s and 6.92 s in the nonstationary and broadband cases, respectively, while the TRESM costs 72.81 s and 71.94 s.

5 Conclusions

To address the time-consuming and instability problems encountered in the time-domain inverse technique for the localization and quantification of rotating sound sources, an improved technique is developed in this paper. In the improved technique, a de-Dopplerization method in the time-domain rotating reference frame is first applied to eliminate the Doppler effect caused by source rotation in the measured pressure signals, and then the restored

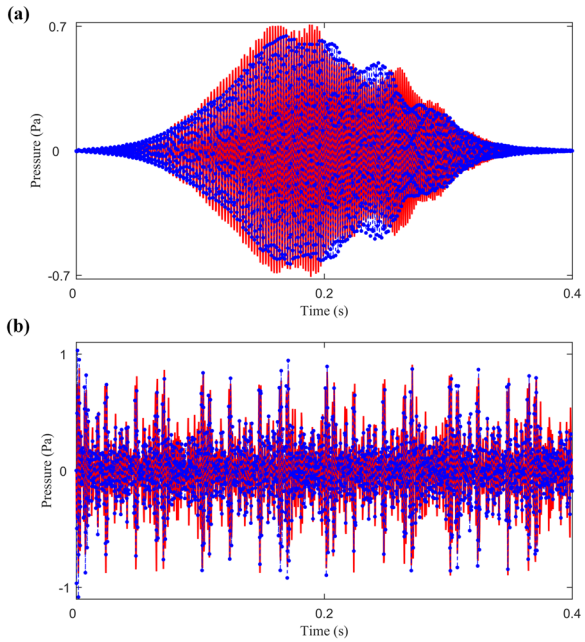

Figure 12 Comparison of the measured pressure (solid lines) and the pressure predicted by using the source strength obtained by the improved technique (dashed lines with solid points) at the reference point of (0.4 m, 3π/2 rad, 0 m) in (**a**) the nonstationary case and (**b**) the broadband case

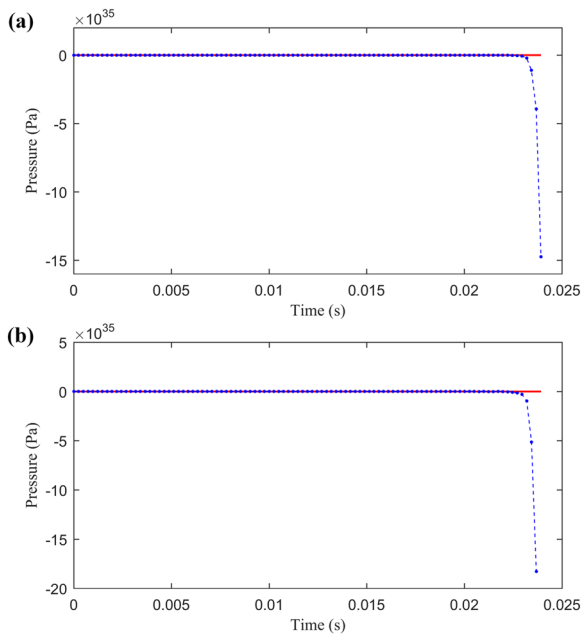

Figure 13 Comparison of the measured pressure (solid lines) and the pressure predicted by using the TRESM (dashed lines with solid points) at the reference point of (0.4 m, 3π/2 rad, 0 m) in (**a**) the nonstationary case and (**b**) the broadband case

pressure signals without the Doppler effect are input to the TSESM to locate and quantify sound sources. Compared with the original one, the improved technique avoids the time-consuming process of solving the transcendental equation at each time step, and facilitates the treatment of the instability problem because the transfer matrix does not change with time. Numerical simulation results showed that the de-Dopplerization method can eliminate the Doppler effect effectively for nonstationary and broadband sources. After eliminating the Doppler effect, the positions and strengths of rotating sound sources were located and quantified accurately by the TSESM. Experiment involving one rotating loudspeaker verified the validity of the de-Dopplerization method and TSESM in both nonstationary and broadband cases. Numerical and experimental results also demonstrated that the improved technique can guarantee a more stable reconstruction and compute more efficiently than the TRESM.

Acknowledgements
Not applicable.

Authors' Contributions
XZ was in charge of the whole trial; XZ wrote the manuscript; YL, YZ, CB assisted with sampling and laboratory analyses; JL, LX revised the manuscript. All authors read and approved the final manuscript.

Authors' Information
Xiaozheng Zhang born in 1985, is currently a professor at *Institute of Sound and Vibration Research, Hefei University of Technology, China*. He received his PhD degree from *Hefei University of Technology, China*, in 2012. His research interests include vibration and noise control.
Yinlong Li born in 1995, is currently an engineer at *Volkswagen (Anhui) Automotive Company Limited, China*. He received his master degree on mechanical manufacture in *Hefei University of Technology, China*, in 2021.
Yongbin Zhang born in 1982, is currently a professor at *Institute of Sound and Vibration Research, Hefei University of Technology, China*. He received his PhD degree from *Hefei University of Technology, China*, in 2008. His research interests include vibration and noise control.
Chuanxing Bi born in 1978, is currently a professor at *Institute of Sound and Vibration Research, Hefei University of Technology, China*. He received his PhD degree from *Hefei University of Technology, China*, in 2004. His research interests include vibration and noise control.
Jinghao Li born in 1992, is currently an engineer at *East China Electric Power Test & Research Institute, China Datang Corporation Science and Technology General Research Institute Co. LTD, Hefei, China*. He received his master degree on Mechanical Engineering from *North China Electric Power University*, China, in 2017.
Liang Xu born in 1981, is currently an associate professor at *Institute of Sound and Vibration Research, Hefei University of Technology, China*. He received his PhD degree from *Hefei University of Technology, China*, in 2009. His research interests include vibration and noise control.

Funding
Supported by National Natural Science Foundation of China (Grant Nos. 51875147, 12174082, 51675149)

Declarations

Competing Interests
The authors declare no competing financial interests.

Received: 6 August 2021 Revised: 25 July 2022 Accepted: 28 September 2023
Published online: 07 November 2023

References

[1] C R Lowis, P Joseph. Determining the strength of rotating broadband sources in ducts by inverse methods. *Journal of Sound and Vibration*, 2006, 295(3–5): 614–632.
[2] C R Lowis, P Joseph. A focused beamformer technique for separating rotor and stator-based broadband sources. *Proceedings of 12th AIAA/CEAS Aeroacoustics Conference*, Cambridge, USA, May 8–10, 2006: 1–14.
[3] W Pannert, C Maier. Rotating beamforming – motion-compensation in the frequency domain and application of high-resolution beamforming algorithms. *Journal of Sound and Vibration*, 2014, 333(7): 1899–1922.
[4] L C Caldas, P C Greco, C C Pagani, et al. Acoustic imaging of in-duct aero-engine noise sources using rotating beamforming and phased arrays. *IEEE Transactions on Computational Imaging*, 2017, 3(3): 485–492.
[5] Z G Chu, S J Yin, Y Yang, et al. Filter-and-sum based high-resolution CLEAN-SC with spherical microphone arrays. *Applied Acoustics*, 2021, 182: 108278-1–108278-9.
[6] Y H Heo, J G Ih, H Bodén. Acoustic source identification of an axial fan in a duct considering the rotation effect. *The Journal of the Acoustical Society of America*, 2016, 140(145): 145–156.
[7] R P Dougherty, B E Walker. Virtual rotating microphone imaging of broadband fan noise. *Proceedings of 15th AIAA/CEAS Aeroacoustics Conference*, Miami, Florida, USA, May 11–13, 2009: 1–14.
[8] S Jekosch, E Sarradj. An extension of the virtual rotating array method using arbitrary microphone configurations for the localization of rotating sound sources. *Acoustics*, 2020, 2: 330–342.
[9] S Jekosch, G Herold, E Sarradj. Virtual rotating array methods for arbitrary micro-phone configurations. *Proceedings of the 8th Berlin Beamforming Conference*, Berlin, Germany, March 2–3, 2020: 1–14.
[10] W Ma, H Bao, C Zhang, et al. Beamforming of phased microphone array for rotating sound source localization. *Journal of Sound and Vibration*, 2020, 467: 115064-1–115064-17.
[11] S Oerlemans, P Sijtsma, B Méndez López. Location and quantification of noise sources on a wind turbine. *Journal of Sound and Vibration*, 2007, 299(4–5): 869–883.
[12] P Sijtsma. Using phased array beamforming to identify broadband noise sources in a turbofan engine. *International Journal of Aeroacoustics*, 2010, 9(3): 357–374.
[13] O Minck, N Binder, O Cherrier, et al. Fan noise analysis using a micro-phone array. *Proceedings of Conference on Fan Noise, Technology, and Numerical Methods*, Senlis, France, April 18–20, 2012: 1–8.
[14] O Amoiridis, A Zarri, R Zamponi, et al. Sound localization and quantification analysis of an automotive engine cooling module. *Journal of Sound and Vibration*, 2022, 517: 116534-1–116534-18.
[15] W Ma, C Zhang. Doppler effect in the time-domain beamforming for rotating sound source identification. *The Journal of the Acoustical Society of America*, 2020, 148(1): 430–443.
[16] X J Pan, H J Wu, W K Jiang. Beamforming correction for the singular problem in identifying rotating sources with non-uniform directivity. *The Journal of the Acoustical Society of America*, 2020, 147(5): 3151–3159.
[17] M Debrouwere, D Angland. Airy pattern approximation of a phased microphone array response to a rotating point source. *The Journal of the Acoustical Society of America*, 2017, 141(2): 1009–1018.
[18] X Zhang, Z G Chu, Y Yang, et al. An alternative hybrid time-frequency domain approach based on fast iterative shrinkage-thresholding algorithm for rotating acoustic source identification. *IEEE Access*, 2019, 7: 59797–59805.
[19] P X Mo, W K Jiang. A hybrid deconvolution approach to separate stationary and moving single-tone acoustic sources by phased microphone array measurements. *Mechanical Systems and Signal Processing*, 2017, 84: 399–413.
[20] N Chu, Q Huang, L Yu, et al. Rotating acoustic source localization: a power propagation forward model and its high-resolution inverse methods. *Measurement*, 2021, 174: 109006-1–109006-18.
[21] N Chu, Q Liu, L Yu, et al. High-resolution localization of rotating acoustic sources: An experimental investigation and axial fan application. *Measurement*, 2022, 196: 111149-1–111149-16.
[22] X Z Zhang, C X Bi, Y B Zhang, et al. A time-domain inverse technique for the localization and quantification of rotating sound sources. *Mechanical Systems and Signal Processing*, 2017, 90: 15–29.
[23] C X Bi, Y Xu, Y B Zhang, et al. A time-domain inverse method for the localization and quantification of unsteady rotating loading sources. *Journal of Sound and Vibration*, 2021, 512: 116405-1–116405-15.
[24] W Kropp, U P Svensson. Time domain formulation of the method of equivalent sources. *Acta Acustica*, 1995, 3: 67–73.
[25] W Kropp, U P Svensson. Application of the time domain formulation of the method of equivalent sources to radiation and scattering problems. *Acustica*, 1995, 81: 528–543.
[26] S Lee, Review: the use of equivalent source method in computational acoustics. *Journal of Computational Acoustics*, 2017, 25(1): 1630001-1–1630001-19.
[27] S Lee, K S Brentner, P J Morris. Acoustic scattering in the time domain using an equivalent source method. *AIAA Journal*, 2010, 48(12): 2772–2780.
[28] S Lee, K S Brentner, P J Morris. Time-domain approach for acoustic scattering of rotorcraft noise. *Journal of the American Helicopter Society*, 2012, 57: 042001-1–042001-12.
[29] X Z Zhang, C X Bi, Y B Zhang, et al. Transient nearfield acoustic holography based on an interpolated time-domain equivalent source method. *The Journal of the Acoustical Society of America*, 2011, 130(3): 1430–1440.
[30] X Z Zhang, C X Bi, Y B Zhang, et al. On the stability of transient nearfield acoustic holography based on the time domain equivalent source method. *The Journal of the Acoustical Society of America*, 2019, 146(2): 1335–1349.